

The catalogue of radial velocity variable hot subluminous stars from the MUCHFUSS project (Corrigendum)

S. Geier^{1,2}, T. Kupfer³, U. Heber², V. Schaffenroth^{2,4}, B. N. Barlow⁵, R. H. Østensen⁶, S. J. O'Toole⁷, E. Ziegerer², C. Heuser², P. F. L. Maxted⁸, B. T. Gänsicke⁹, T. R. Marsh⁹, R. Napiwotzki¹⁰, P. Brünnner², M. Schindewolf², and F. Niederhofer¹

¹ European Southern Observatory, Karl-Schwarzschild-Str. 2, 85748 Garching, Germany
e-mail: sgeier@eso.org

² Dr. Karl Remeis-Observatory & ECAP, Astronomical Institute, Friedrich-Alexander University Erlangen-Nuremberg, Sternwartstr. 7, 96049 Bamberg, Germany

³ Department of Astrophysics/IMAPP, Radboud University Nijmegen, PO Box 9010, 6500 GL Nijmegen, The Netherlands

⁴ Institute for Astro- and Particle Physics, University of Innsbruck, Technikerstr. 25/8, 6020 Innsbruck, Austria

⁵ Department of Physics, High Point University, One University Parkway, High Point, NC 27268, USA

⁶ Institute of Astronomy, KU Leuven, Celestijnenlaan 200D, 3001 Heverlee, Belgium

⁷ Australian Astronomical Observatory, PO Box 915, North Ryde NSW 1670, Australia

⁸ Astrophysics Group, Keele University, Staffordshire, ST5 5BG, UK

⁹ Department of Physics, University of Warwick, Coventry CV4 7AL, UK

¹⁰ Centre of Astrophysics Research, University of Hertfordshire, College Lane, Hatfield AL10 9AB, UK

A&A 577, A26 (2015), DOI: [10.1051/0004-6361/201525666](https://doi.org/10.1051/0004-6361/201525666)

Key words. binaries: spectroscopic – subdwarfs – stars: horizontal branch – stars: atmospheres – errata, addenda

The function we used to calculate the logarithm of the false-detection probability provides the natural logarithm $\ln p$ and not the decadal logarithm as incorrectly assumed in the paper. This mildly affects the number of radial velocity (RV) variable stars and significantly the number of RV variable candidates in our sample. The conclusions of the paper essentially remain the same.

We consider the detection of RV variability to be significant, if the false-detection probability p is smaller than 0.01% ($\ln p < -9.2$). The fraction of such significant detections in our initial sample of 196 is now 39% (76 objects). Objects with false-detection probabilities between 0.01% and 5% ($\ln p = -9.2$ to $\ln p = -3.0$) are regarded as candidates for RV variability and constitute 27% of the initial sample (53 objects). About 34% ($\ln p > -3.0$, 67 objects) are regarded as non-detections. Removing those non-detections we end up with a sample of 129 stars, which show RV variability with probabilities between 95% and 99.9% (see Table 1).

Tables 3–5 and A.1 as well as Figures 1–6 of the original paper have been updated (Tables 2–5, Figs. 1–4).

The corrected upper limit for the fraction of extremely close binary sdB+NS/BH binaries is 1.5% instead of 1.3%.

The RV-variable sample now contains 18 helium-rich hot subdwarf stars. 6 of them show significant RV variations while 12 qualify as candidates (see Table 3). The He-sdOB J160450.44+051909.2 discussed in the paper is not regarded as RV-variable candidate any more.

Table 1. Sample statistics.

Class	RV variable	RV variable candidates	Non-detections
H-rich sdO/B	65	36	51
He-rich sdO/B	6	12	11
Others	5	5	5
Total	76	53	67

References

- Althaus, L. G., Panei, J. A., Miller Bertolami, M. M., et al. 2009, [ApJ, 704, 1605](https://doi.org/10.1088/0004-637X/704/1/1605)
Dorman, B., Rood, R. T., & O'Connell, R. W. 1993, [ApJ, 419, 596](https://doi.org/10.1086/173000)
Driebe, T., Schönberner, D., Bloecker, T., & Hervig, F. 1998, [A&A, 339, 123](https://doi.org/10.1051/0004-6361/19980123)
Geier, S., Hirsch, H., Tillich, A., et al. 2011a, [A&A, 530, A28](https://doi.org/10.1051/0004-6361/201116428)
Geier, S., Maxted, P. F. L., Napiwotzki, R., et al. 2011b, [A&A, 526, A39](https://doi.org/10.1051/0004-6361/201116439)
Geier, S., Schaffenroth, V., Drechsel, H., et al. 2011c, [ApJ, 731, L22](https://doi.org/10.1088/0004-637X/731/2/L22)
Kupfer, T., Geier, S., Schaffenroth, V., et al. 2015, [A&A, 576, A44](https://doi.org/10.1051/0004-6361/201525666)
Østensen, R. H., Geier, S., Schaffenroth, V., et al. 2013, [A&A, 559, A35](https://doi.org/10.1051/0004-6361/201321950)
Schaffenroth, V., Geier, S., Heber, U., et al. 2014, [A&A, 564, A98](https://doi.org/10.1051/0004-6361/201423800)
Reindl, N., Geier, S., Kupfer, T., et al. 2016, [A&A, 587, A101](https://doi.org/10.1051/0004-6361/201628777)
Schaller, G., Schaerer, D., Meynet, G., & Maeder, A. 1992, [A&AS, 96, 269](https://doi.org/10.1088/0004-6256/96/2/269)
Schönberner, D. 1983, [ApJ, 272, 708](https://doi.org/10.1088/0004-637X/272/2/708)
Werner, K., Rauch, T., & Kepler, S. O. 2014, [A&A, 564, A53](https://doi.org/10.1051/0004-6361/201423800)

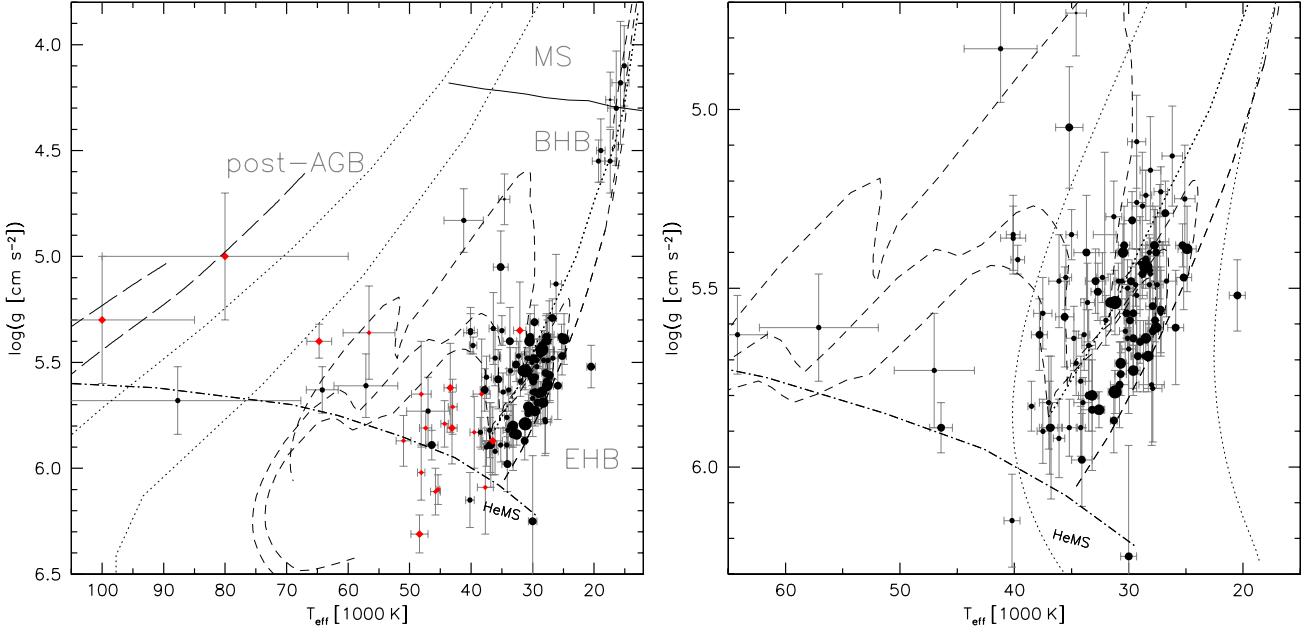


Fig. 1. Left panel: $T_{\text{eff}} - \log g$ diagram of the full sample of hot, subluminous, RV-variable stars. The size of the symbols scales with ΔRV_{max} . The black circles mark stars with hydrogen dominated atmospheres ($\log y < 0$), while the red diamonds mark stars with helium dominated atmospheres. The helium main sequence (HeMS) and the HB band are superimposed with HB evolutionary tracks (dashed lines) for subsolar metallicity ($\log z = -1.48$) from Dorman et al. (1993). The three tracks in the high temperature range correspond to helium core masses of 0.488, 0.490 and $0.495 M_{\odot}$ (from bottom-left to top-right). Those tracks mark the EHB evolution, since the stars do not reascend the giant branch in the helium shell-burning phase. The two tracks in the upper right correspond to core masses of 0.53 and $0.54 M_{\odot}$. Blue horizontal branch stars following those tracks are expected to experience a second giant phase. The solid line marks the relevant part of the zero-age main sequence for solar metallicity taken from Schaller et al. (1992). The two dotted lines are post-AGB tracks for hydrogen-rich stars with masses of 0.546 (lower line) and $0.565 M_{\odot}$ (upper line) taken from Schönberner (1983). The two long-dashed lines are post-AGB tracks for helium-rich stars with masses of 0.53 (lower line) and $0.609 M_{\odot}$ (upper line) taken from Althaus et al. (2009). Right panel: $T_{\text{eff}} - \log g$ diagram of RV variable hydrogen-rich sdB and sdOB stars. The two dotted lines mark post-RGB tracks (Driebe et al. 1998) for core masses of 0.234 (left) and $0.259 M_{\odot}$ (right).

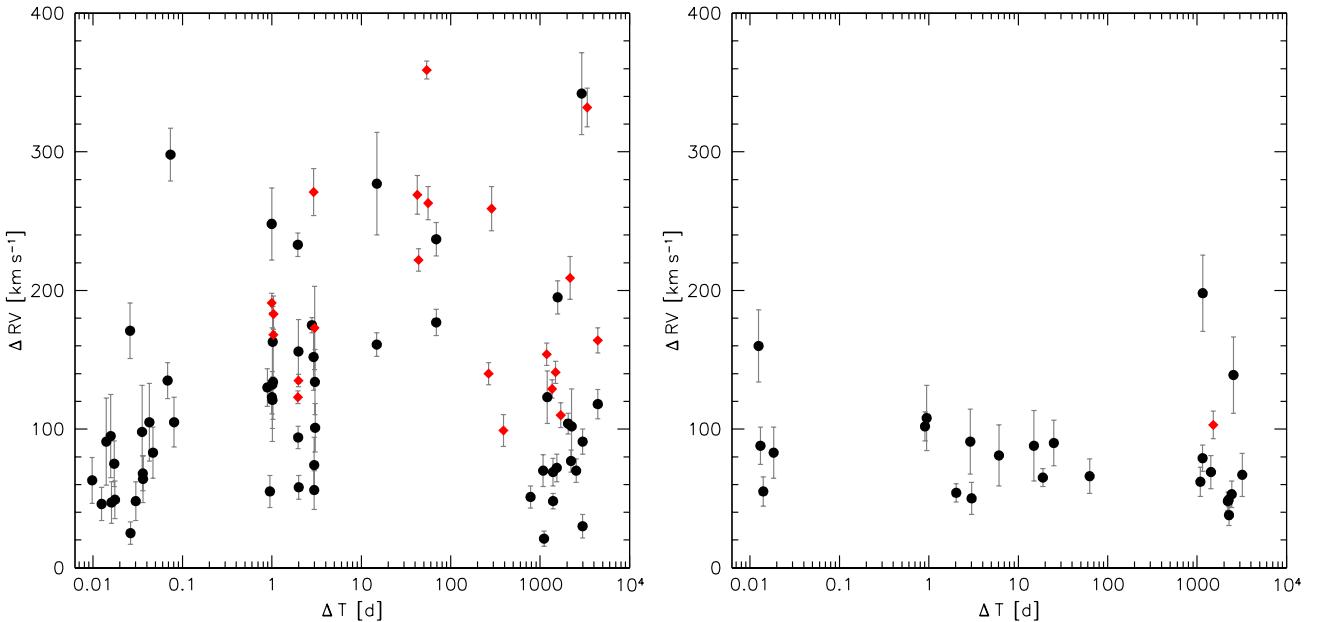


Fig. 2. Left panel: highest RV shift between individual spectra plotted against time difference between the corresponding observing epochs. The filled red diamonds mark sdB binaries with known orbital parameters (Kupfer et al. 2015), while the filled black circles mark the rest of the hydrogen-rich sdB sample of RV variable stars. Right panel: the same plot for the hydrogen-rich sdOB and sdO sample of RV variable stars.

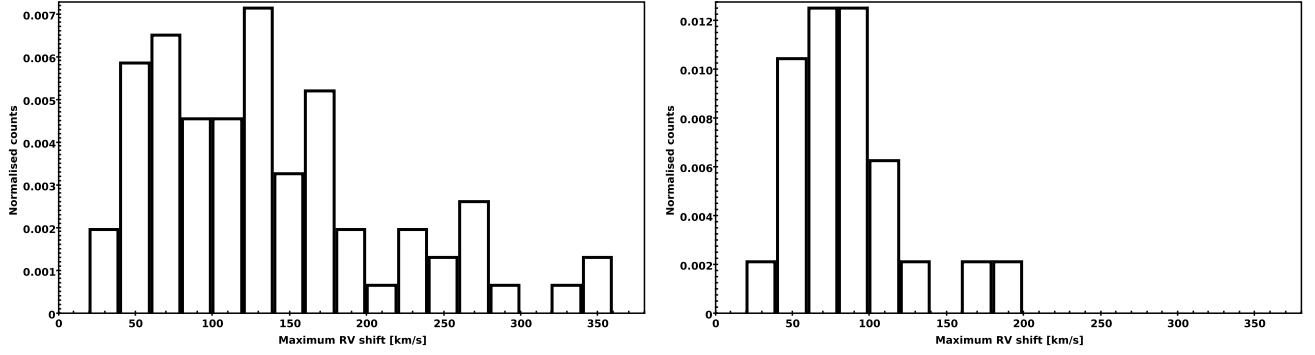


Fig. 3. ΔRV_{\max} distribution of RV-variable sdB stars (left panel) as well as sdOB and sdO stars with hydrogen-rich atmospheres (right panel).

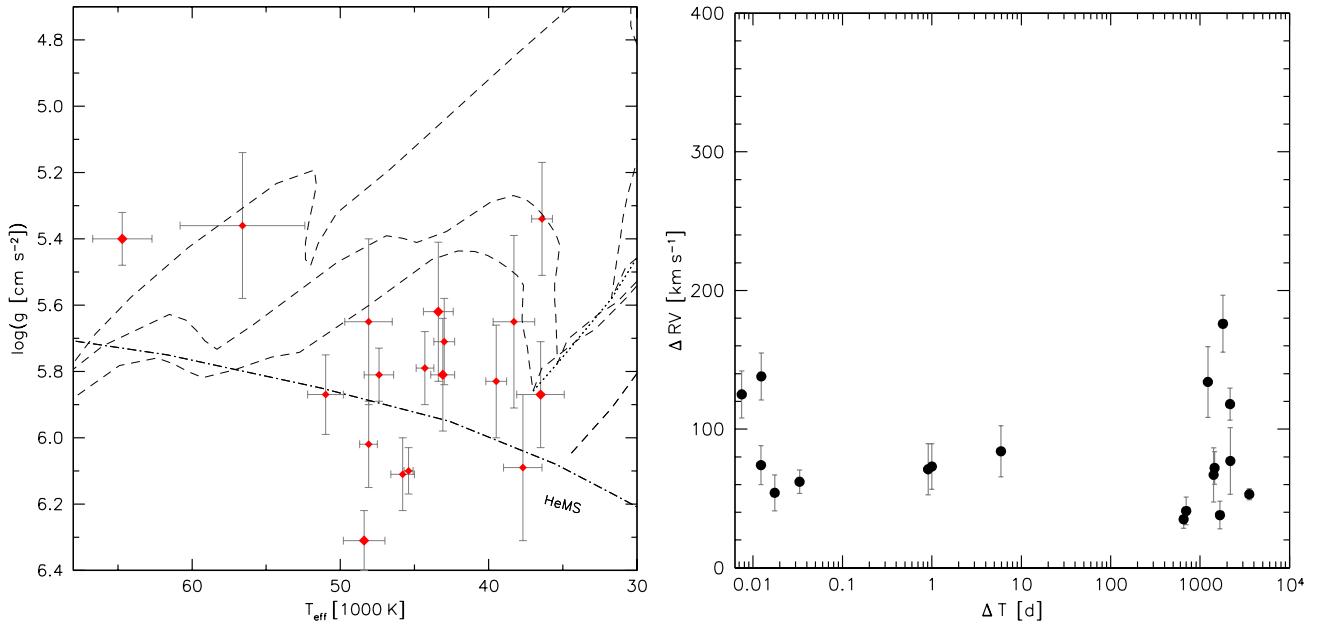


Fig. 4. Left panel: $T_{\text{eff}} - \log g$ diagram of RV variable helium-rich sdOB and sdO stars (see Fig. 1). The size of the symbols scales with ΔRV_{\max} . The helium main sequence (HeMS) and the HB band are superimposed with HB evolutionary tracks (dashed lines) for subsolar metallicity ($\log z = -1.48$) from Dorman et al. (1993). The three tracks correspond to helium core masses of $0.488, 0.490$ and $0.495 M_{\odot}$ (from bottom-left to top-right). Right panel: highest RV shift between individual spectra plotted against time difference between the corresponding observing epochs for helium-rich sdO and sdOB stars (see Fig. 2).

Table 2. continued.

Name	Class	m_V [mag]	T_{eff} [K]	$\log g$	$\log y$	d [kpc]	Δt [d]	ΔRV_{max} [km s $^{-1}$]	N	$\ln p$
J074534.16+372718.5 ^a	sdB	17.9	37 500 \pm 500	5.90 \pm 0.09	<−3.0	4.6 $^{+0.5}_{-0.5}$	0.0363	64.0 \pm 17.0	8	−9.74
J202313.83+131254.9 ^a	sdB	17.2	29 600 \pm 600	5.64 \pm 0.14	−2.1 \pm 0.1	3.8 $^{+0.7}_{-0.6}$	1201.7981	123.0 \pm 19.0	5	−9.20
J162610.34+130401.6	sdB	19.4	33 900 \pm 500	5.63 \pm 0.10	−1.0 \pm 0.1	12.1 $^{+1.7}_{-1.5}$	780.7541	51.0 \pm 8.0	3	−9.16
J030607.95+382335.7 ⁱ	sdO	16.8	30 100 \pm 300	5.64 \pm 0.03	−2.1 \pm 0.1	3.2 $^{+0.1}_{-0.1}$	2210.7452	48.0 \pm 6.5	8	−8.85
J204451.08−062753.8	sdO	20.0	57 100 \pm 5200	5.61 \pm 0.15	−2.2 \pm 0.4	21.4 $^{+5.1}_{-4.2}$	1087.0571	62.0 \pm 10.5	3	−7.88
J091615.49+132833.1	sdB	17.5	30 900 \pm 400	5.48 \pm 0.05	<−3.0	5.4 $^{+0.4}_{-0.4}$	0.9512	55.0 \pm 11.5	3	−7.58
J163413.09+163109.5	sdB	18.3	34 600 \pm 900	4.73 \pm 0.12	−2.0 \pm 0.5	20.7 $^{+3.5}_{-3.1}$	1105.3751	21.0 \pm 5.5	3	−7.44
J123220.09+260913.3	sdB	18.1	33 700 \pm 1100	5.40 \pm 0.16	−1.3 \pm 0.2	8.5 $^{+2.0}_{-1.7}$	1.0302	134.0 \pm 27.0	5	−7.36
J185129.02+182358.8	sdB	16.8	27 800 \pm 700	5.38 \pm 0.10	<−3.0	3.9 $^{+0.6}_{-0.5}$	0.0808	105.0 \pm 18.0	22	−7.33
J220048.67+123612.4 ^h	sdO	18.6	64 200 \pm 2600	5.63 \pm 0.11	−1.3 \pm 0.1	11.4 $^{+1.8}_{-1.6}$	2437.2535	53.0 \pm 9.5	3	−7.04
J153752.95+160201.8	sdB	18.4	32 300 \pm 500	5.47 \pm 0.07	<−3.0	8.5 $^{+0.9}_{-0.8}$	0.0361	68.0 \pm 12.5	3	−7.03
J183229.22+402418.4	sdO	15.7	40 100 \pm 600	5.35 \pm 0.11	−2.0 \pm 0.2	3.3 $^{+0.5}_{-0.4}$	3.0098	50.0 \pm 11.5	5	−6.82
J181126.83+233413.7	sdB	18.4	—	—	—	—	1.0156	121.0 \pm 20.5	7	−6.47
J204448.63+153638.8 ^a	sdB	17.9	29 600 \pm 600	5.57 \pm 0.09	−2.2 \pm 0.1	5.7 $^{+0.7}_{-0.7}$	3.0489	101.0 \pm 17.5	7	−6.41
J185414.11+175200.2	sdOB	16.9	35 200 \pm 700	5.89 \pm 0.08	−1.4 \pm 0.1	2.9 $^{+0.3}_{-0.3}$	6.0874	81.0 \pm 22.0	10	−6.25
J171629.92+575121.2 ^a	sdOB	18.2	37 500 \pm 800	5.57 \pm 0.10	<−0.7	7.8 $^{+1.0}_{-0.9}$	3195.9096	67.0 \pm 15.5	12	−6.14
J184434.74+412158.7	sdB	17.3	27 200 \pm 500	5.57 \pm 0.12	−2.6 \pm 0.1	4.0 $^{+0.7}_{-0.6}$	2.9795	56.0 \pm 14.0	5	−5.72
J091136.73+124015.2	sdB	18.2	—	—	—	—	0.0173	75.0 \pm 16.5	3	−5.31
J151337.80+195012.5	sdB	18.9	—	—	—	—	0.0354	98.0 \pm 33.5	4	−5.16
J172727.55+091215.5 ⁱ	sdO	17.5	40 100 \pm 1100	5.36 \pm 0.09	<−2.1	7.4 $^{+0.9}_{-0.8}$	0.0141	55.0 \pm 10.5	6	−5.10
J112242.69+613758.5 ^a	sdB	15.4	29 300 \pm 500	5.69 \pm 0.10	−2.3 \pm 0.3	1.5 $^{+0.2}_{-0.2}$	0.0469	83.0 \pm 18.5	6	−5.08
J161140.50+201857.0 ^a	sdOB	18.5	36 900 \pm 700	5.89 \pm 0.13	−1.2 \pm 0.1	6.1 $^{+1.1}_{-0.9}$	0.9472	108.0 \pm 23.5	5	−4.77
J065044.30+383133.7	sdOB	17.3	34 200 \pm 400	5.76 \pm 0.07	−2.9 \pm 0.2	3.9 $^{+0.4}_{-0.3}$	0.0131	88.0 \pm 13.5	14	−4.63
J170645.57+243208.6 ^a	sdB	17.8	32 000 \pm 500	5.59 \pm 0.07	<−4.0	5.5 $^{+0.6}_{-0.5}$	0.0125	46.0 \pm 12.0	3	−4.41
J083359.65−043521.9	sdOB	18.3	36 100 \pm 500	5.92 \pm 0.11	−1.9 \pm 0.2	5.5 $^{+0.8}_{-0.7}$	14.9765	88.0 \pm 25.5	11	−4.39
J140545.25+014419.0 ^a	sdB	15.8	27 300 \pm 800	5.37 \pm 0.16	−1.9 \pm 0.2	2.5 $^{+0.6}_{-0.5}$	0.0263	25.0 \pm 8.0	3	−4.12
J160534.96+062733.5	sdB	19.3	—	—	—	—	1.0113	132.0 \pm 41.0	8	−3.97
J221920.67+394603.5	sdO	17.3	47 000 \pm 3500	5.73 \pm 0.16	<−3.0	4.7 $^{+1.2}_{-0.9}$	62.8679	66.0 \pm 12.5	8	−3.93
J183840.52+400226.8	sdB	17.8	29 300 \pm 900	5.52 \pm 0.13	−1.6 \pm 0.2	5.5 $^{+1.1}_{-0.9}$	2.9795	74.0 \pm 20.0	5	−3.89
J115716.37+612410.7 ^a	sdB	17.2	29 900 \pm 500	5.59 \pm 0.08	−3.2 \pm 0.8	4.0 $^{+0.5}_{-0.4}$	2250.6902	102.0 \pm 27.0	7	−3.63
J113303.70+290223.0 ^a	sDB/DA	18.9	—	—	—	—	0.0158	95.0 \pm 30.0	3	−3.39
J161817.65+120159.6 ^a	sdB	18.0	32 100 \pm 1000	5.35 \pm 0.23	< 0.0	8.1 $^{+2.8}_{-2.1}$	0.0427	105.0 \pm 28.0	4	−3.35
J205101.72+011259.7	sDB+X	17.6	—	—	—	—	0.0141	91.0 \pm 31.5	8	−3.28
J133638.81+111949.4 ^a	sdB	17.3	27 500 \pm 500	5.49 \pm 0.08	−2.7 \pm 0.2	4.4 $^{+0.5}_{-0.5}$	0.0301	48.0 \pm 14.0	3	−3.25
J094044.07+004759.6 ^h	sdB	19.1	37 000 \pm 800	5.82 \pm 0.13	−0.1 \pm 0.1	8.8 $^{+1.5}_{-1.3}$	2982.7971	30.0 \pm 8.5	2	−3.24
J210454.89+110645.5 ^a	sdOB	17.3	37 800 \pm 700	5.63 \pm 0.10	−2.4 \pm 0.2	4.9 $^{+0.6}_{-0.6}$	2548.0064	139.0 \pm 27.5	9	−3.14
J211651.96+003328.5 ^a	sdB	18.0	27 900 \pm 800	5.78 \pm 0.15	−3.9 \pm 0.7	4.3 $^{+0.9}_{-0.8}$	0.0161	47.0 \pm 15.0	3	−3.08
J091428.87+125023.8	sdB	18.0	33 600 \pm 600	5.54 \pm 0.11	<−3.0	7.0 $^{+1.1}_{-0.9}$	0.0176	49.0 \pm 13.5	3	−3.07

Table 3. Parameters of 18 helium-rich hot subdwarfs (6 RV variable, 12 RV variable candidates).

Name	Class	m_V [mag]	T_{eff} [K]	$\log g$	$\log y$	d [kpc]	Δt [d]	ΔRV_{max} [km s $^{-1}$]	N	$\ln p$
J232757.46+483755.2 ^a	He-sdO	15.8	64 700 \pm 2000	5.40 \pm 0.08	>+2.0	4.2 $^{+0.5}_{-0.4}$	1799.6136	176.0 \pm 20.5	59	-680.31
J141549.05+111213.9 ^a	He-sdO	16.1	43 100 \pm 800	5.81 \pm 0.17	>+2.0	2.4 $^{+0.5}_{-0.4}$	0.0075	125.0 \pm 17.0	35	-86.42
J103549.68+092551.9 ^a	He-sdO	16.3	48 100 \pm 600	6.02 \pm 0.13	>+2.0	2.2 $^{+0.4}_{-0.3}$	3541.9636	53.0 \pm 4.0	6	-54.25
J170045.09+391830.3	He-sdOB	18.2	36 500 \pm 1600	5.87 \pm 0.16	+0.1 \pm 0.1	5.5 $^{+1.2}_{-1.0}$	2160.0414	118.0 \pm 11.5	10	-44.76
J161014.87+045046.6	He-sdO	17.3	48 400 \pm 1400	6.31 \pm 0.09	>+2.0	2.5 $^{+0.3}_{-0.3}$	0.0124	138.0 \pm 17.0	14	-31.77
J110215.45+024034.1 ^a	He-sdO	17.5	56 600 \pm 4200	5.36 \pm 0.22	>+2.0	8.9 $^{+3.0}_{-2.2}$	0.0332	62.0 \pm 8.5	3	-10.91
J174516.32+244348.3 ^a	He-sdO	17.7	43 400 \pm 1000	5.62 \pm 0.21	>+2.0	6.2 $^{+1.8}_{-1.4}$	1220.5806	134.0 \pm 25.5	13	-8.81
J160304.07+165953.8 ^b	He-sdO	16.9	45 400 \pm 300	6.10 \pm 0.07	>+2.0	2.5 $^{+0.2}_{-0.2}$	0.9087	71.0 \pm 18.5	5	-8.11
J094856.95+334151.0 ^a	He-sdO	17.7	51 000 \pm 1200	5.87 \pm 0.12	+1.8 \pm 0.5	5.1 $^{+0.8}_{-0.7}$	0.0123	74.0 \pm 14.0	3	-7.73
J152136.25+162150.3	He-sdO	17.1	47 400 \pm 1000	5.81 \pm 0.08	+1.6 \pm 0.4	4.0 $^{+0.4}_{-0.4}$	2175.9687	77.0 \pm 24.0	9	-5.94
J163416.08+221141.0	He-sdOB	15.5	38 300 \pm 1400	5.65 \pm 0.26	>+2.0	2.0 $^{+0.8}_{-0.6}$	653.3309	35.0 \pm 6.5	6	-5.55
J153237.94+275636.9	He-sdO	18.5	37 700 \pm 1300	6.09 \pm 0.22	+0.0 \pm 0.2	5.0 $^{+1.5}_{-1.2}$	1.0012	73.0 \pm 16.5	3	-5.52
J233914.00+134214.3	He-sdO	17.6	48 100 \pm 1600	5.65 \pm 0.25	>+2.0	6.0 $^{+2.1}_{-1.6}$	1451.6391	72.0 \pm 11.8	12	-5.11
J173034.09+272139.8 ^c	He-sdO	18.9	39 500 \pm 700	5.83 \pm 0.17	+0.1 \pm 0.1	8.1 $^{+1.8}_{-1.5}$	698.7112	41.0 \pm 10.0	2	-5.00
J170214.00+194255.1 ^b	He-sdO	15.8	44 300 \pm 600	5.79 \pm 0.11	>+2.0	2.1 $^{+0.3}_{-0.3}$	1665.2088	38.0 \pm 10.0	5	-3.76
J081329.81+383326.9	He-sdO	17.5	45 800 \pm 800	6.11 \pm 0.11	+1.8 \pm 0.4	3.3 $^{+0.5}_{-0.4}$	0.0175	54.0 \pm 13.0	6	-3.35
J204940.85+165003.6 ^a	He-sdO	17.9	43 000 \pm 700	5.71 \pm 0.13	>+2.0	6.2 $^{+1.1}_{-0.9}$	5.9325	84.0 \pm 18.5	7	-3.13
J160623.21+363005.4	He-sdOB	18.5	36 400 \pm 700	5.34 \pm 0.17	-0.5 \pm 0.1	11.3 $^{+2.6}_{-2.1}$	1414.9811	67.0 \pm 19.5	2	-3.04

Notes. ^(a) Atmospheric parameters taken from Geier et al. (2011a). ^(b) Atmospheric parameters derived from a spectrum taken with ESO-VLT/FORS1. ^(c) Atmospheric parameters derived from a spectrum taken with WHT/ISIS.

Table 4. Parameters of 10 other types of hot stars (5 RV variable, 5 RV variable candidates).

Name	Class	m_V [mag]	T_{eff} [K]	$\log g$	$\log y$	d [kpc]	Δt [d]	ΔRV_{max} [km s $^{-1}$]	N	$\ln p$
J131916.15-011404.9	BHB	16.4	17 400 \pm 800	4.55 \pm 0.15	-1.9 \pm 0.2	5.9 $^{+1.4}_{-1.1}$	2888.0925	46.0 \pm 9.0	8	-42.10
J164121.22+363542.7	BHB	17.4	19 300 \pm 1000	4.55 \pm 0.10	-1.9 \pm 0.2	9.9 $^{+1.7}_{-1.4}$	1035.9093	99.0 \pm 9.0	8	-39.13
J075732.18+184329.3 ^a	O(He)	18.6	80 000 \pm 2000	5.00 \pm 0.30	>+2.0	29.6 $^{+12.7}_{-9.0}$	0.0216	107.0 \pm 22.0	6	-30.13
J155610.40+254640.3 ^b	PG 1159	17.9	100 000 $^{+15000}_{-10000}$	5.3 \pm 0.3	>+2.0	16.9 $^{+8.9}_{-5.6}$	231.1694	116.0 \pm 21.0	10	-17.98
J201302.58-105826.1	MS-B	18.5	16 400 \pm 1400	4.30 \pm 0.27	-1.3 \pm 0.2	51.8 $^{+23.6}_{-16.4}$	2.0155	61.0 \pm 11.5	8	-13.42
J093521.39+482432.4	O(H)	18.5	87 700 \pm 20000	5.68 \pm 0.16	-1.0 \pm 0.3	12.0 $^{+3.7}_{-3.3}$	2269.7542	38.0 \pm 7.5	2	-6.97
J161253.21+060538.7	MS-B	15.5	15 700 \pm 1400	4.18 \pm 0.29	-1.0 \pm 0.2	14.4 $^{+7.2}_{-4.8}$	811.5968	38.0 \pm 7.0	10	-6.84
J020531.40+134739.8 ^c	BHB	18.4	17 400 \pm 700	4.26 \pm 0.13	-1.7 \pm 0.2	20.3 $^{+4.0}_{-3.4}$	2781.1087	28.0 \pm 7.0	3	-3.64
J144023.58+135454.7	BHB	18.3	18 900 \pm 700	4.50 \pm 0.15	-1.9 \pm 0.3	16.1 $^{+3.6}_{-3.0}$	0.0528	78.0 \pm 24.0	4	-3.15
J171947.87+591604.2	MS-B	16.9	15 100 \pm 600	4.10 \pm 0.19	-0.9 \pm 0.2	29.2 $^{+8.3}_{-6.5}$	2568.7218	32.0 \pm 6.5	10	-3.11

Notes. ^(a) Atmospheric parameters taken from Werner et al. (2014). ^(b) Atmospheric parameters taken from Reindl et al. (2016). ^(c) Atmospheric parameters derived from a spectrum taken with ESO-VLT/FORS1.

